International Journal of Power Electronics and Drive System (IJPEDS)
Vol. 17, No. 1, March 2026, pp. 533~552
ISSN: 2088-8694, DOI: 10.11591/ijpeds.v17.i1.pp533-552

A three isolated port DC/DC converter for an energy storage system for renewable energy applications

Faruk Ahmeti[1], Dimitar Arnaudov[1], Sabrije Osmanaj[2]
[1]Department of Power Electronics, Faculty of Electronic Engineering and Technology, Technical University of Sofia, Sofia, Bulgaria
[2]Department of Electronics, Faculty of Electrical and Computer Engineering, University of Pristina, Pristina, Republic of Kosovo

Article Info

Article history:

Received Dec 17, 2024
Revised Dec 4, 2025
Accepted Dec 11, 2025

Keywords:

Bidirectional converters
DC/DC converters
Energy storage
Energy transferring
Resonant converters

ABSTRACT

The use of renewable energy sources like solar photovoltaic, wind, and fuel cells is gaining popularity due to growing environmental awareness, technological advancements, and declining production costs. Power electronic converters are usually used to convert the power from renewable sources to match the load demand and grid requirements. Among these, DC–DC converters are essential for improving system functionality and power density, especially in low-voltage renewable systems that require high voltage gain. This paper presents a systematic evaluation of five advanced DC–DC converter topologies: multi-port DC, boost multiport interleaved step-up, isolated bidirectional, voltage/current fed, and general resonant focusing on their structural complexity, component count, and potential application scenarios. In addition, a novel high-gain three-port resonant A DC–DC converter is proposed, incorporating galvanic isolation via a three-winding high-frequency transformer. The converter adopts a half-bridge resonant inverter and rectifier-based load port, resulting in a compact and cost-effective solution. A detailed analysis of the converter's operation, design considerations, and control strategy is conducted using PLECS simulation. Furthermore, an experimental setup is developed to validate the converter's practical feasibility. The setup schematic and comprehensive comparative tables are included to support the evaluation and highlight the proposed design's capabilities.

Corresponding Author:

Sabrije Osmanaj
Department of Electronics, Faculty of Electrical and Computer Engineering, University of Pristina
Pristina, Republic of Kosovo
Email: sabrije.osmanaj@uni-pr.edu

1. INTRODUCTION

Renewable energy sources, including solar panels, fuel cells, and wind turbines, have attracted ongoing interest due to the world's increasing energy crisis, the depletion of its resources, and greenhouse gas reduction initiatives [1], [2]. However, depending on the temperature and weather, renewable energy sources are irregular and unreliable due to these and other environmental conditions. Batteries and other energy storage systems are used to ensure stability and continuity of the power supply. They can be connected to a common system using multiple single-port converters or a single multi-port converter [3]. In recent years, the use of distributed photovoltaic systems with medium and high power has increased significantly. To increase efficiency, these systems are combined with energy storage systems. Various configurations of hybrid systems based on photovoltaic sources are known in the literature. Bidirectional DC-DC converters are used in hybrid systems. Bidirectional DC-DC converters provide charging and discharging of energy storage systems. Since there may be times when there is not enough energy available from photovoltaics, and energy

from the storage system can be used, it is necessary to have a multi-port converter. From the point of view of ensuring safe operation, the system housings are connected to ground. Galvanically isolated DC-DC converters are used to match the different potentials [4]-[6]. The main disadvantages of having multiple converters in the system are multiple energy conversions and a large number of components. This, in turn, leads to a reduction in efficiency, as well as an increase in size, a decrease in reliability, and an increase in cost. Multi-port converters are used in systems that include wind turbines, fuel cells, and photovoltaic systems [7]. Recently, the three-port DC-DC converters with the configuration shown in Figure 1 have been studied to integrate the renewable energy and energy storage converters into one converter with two inputs. One three-port DC-DC converter can accept two inputs: one input is for the DC output of the PV, and the second DC input, which is a bidirectional port, is for the energy storage system for charging and discharging.

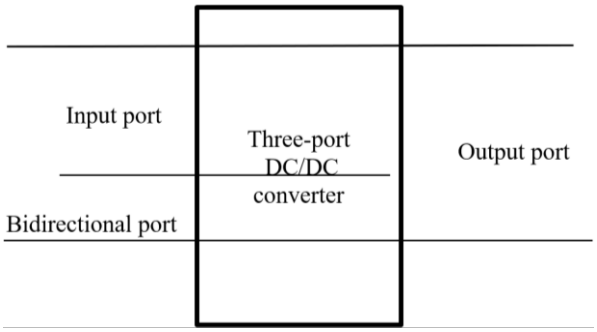

Figure 1. The typical structure of a three-port converter

The output of the three-port DC-DC converter can be connected to the DC load directly or to the grid or AC load by an inverter through a DC link capacitor. Many three-port DC-DC converters, which can satisfy the MPPT and energy-storage charging and discharging requirements, have been reported in the literature. These converters can be categorized into 3 types: non-isolated [8], partly isolated [9], and isolated converters [10].

Non-isolated three-port converters have a structure with fewer components and a simpler design of the magnetic components [11]-[19]. In this case, techniques for achieving soft switching can be used, which are applicable to non-isolated galvanic applications [8], [9]. Another disadvantage of the non-isolated three-port converters is that most of these converters have a limited voltage gain since the freedom of modulation of the voltage conversion ratio is only the duty cycle. Some reported papers use coupled-inductors to extend the voltage conversion ratio to overcome this issue [20]-[22]. Compared to the non-isolated three-port converters, partly isolated three-port converters, which use a transformer to isolate one port from the other two common-grounded ports, can obtain higher voltage gain with a larger turns ratio of the transformer. However, the energy storage system in these converters continues operating in all operating modes, which can shorten the lifespan of the energy system and lower the reliability of the overall system [23]. When using a high-frequency transformer, it is easier to achieve voltage matching between the sources connected to the individual ports [19]. However, the number of components used in this kind of converter is very large since the components are not often shared [9]. Although both partly isolated and isolated converters can be operated with soft switching on the switches using appropriate control and modulation methods, high power loss may still occur due to the leakage inductance of the transformer [23]. Also, the use of a transformer may make the converter bulky and reduce the overall power density.

In most situations, three port converters consist of several full/half-bridge converters and rectifiers, and all three ports are isolated from one another using one or two transformers [24]-[27]. The more independent converters we have in this three-port system, the easier it is to control energy flows, and it is possible to achieve more complex algorithms for controlling flows throughout the system. In a three-port system, it is possible to ensure that when energy is transferred between two of the ports, the third port is not active. When using a high-frequency transformer and a wide range of gain changes during energy transfer, the efficiency coefficient may be reduced as a result of losses in the transformer when operating at different frequencies. However, there is a barrier to the widespread promotion of these clean energy sources because of the intermittent character of renewable sources and the unpredictable nature of load demand. In order to address the challenges of intermittent renewable energy and unpredictable load, power electronic converters with energy storage systems are typically used to convert PV panel output power to match load demand,

improve the dynamic and steady-state characteristics of green generation systems, provide MPPT control, and integrate the energy storage system. The conventional method involves connecting the renewable energy source to the load through a traditional DC-DC converter. Following this, the energy storage system is connected to the input or output port of the conventional DC-DC converter via a bidirectional DC-DC converter for charging and discharging. Due to the additional converter needed for the energy storage system, the primary drawback of these conventional methods is their low efficiency. Furthermore, the multi-stage architecture might lead to a larger unit, a lower power density, and a comparatively higher price [28]-[30].

Applications requiring the integration of various distinct input energy source types, such as fuel cells, wind turbines, and solar PV, can be satisfied by using a multi-input converter. With a single-stage approach, this kind of converter can supply the required power for the load; however, since these multi-input converters lack an energy storage system, the system might not be able to supply the required load demand in situations where the output power exceeds the input power. This can occur during fuel cell operation if there is a sudden rise in load and the fuel cell's chemical reaction cannot keep up with the increase in load quickly enough [31]. When using full-bridge converters, it is easier to obtain symmetrical current waveforms and bidirectional energy transfer, but the control system for controlling the direction of energy flows becomes more complex [32]. Schematic configuration solutions that have been applied to hybrid systems with hydrogen fuel cells can also be applied to other hybrid systems, such as those with photovoltaics. After the introduction of this converter, it has gained a lot of attention from other researchers, in terms of the analysis of the performances of the converter, the control methods, the loss evaluations, and its applications [33]-[40]. To reduce the ripples of the input current, an inductor has been added between the input source and the full-bridge structure in the input port [41]. A new full-bridge-based three-port DC-DC converter is reported in [42]. Compared to that converter, this converter includes two additional series resonant circuits in the primary side of the transformer, to implement the soft switching of the switches to reduce the switching losses. Another benefit of this converter over the previous one is that this converter can operate with a high switching frequency with realizable component values [43]-[46].

2. METHOD AND EXPERIMENTAL IMPLEMENTATION

The proposed three-port DC/DC converter used a topology with two pairs of limiting diodes. This three-port converter's topology consists of three ports that are physically and electrically isolated by a three-winding high-frequency electrical transformer. The first port has an LLC resonant tank and dual limiting diodes coupled with dual MOSFET half-bridge transistors opposite each other, which serve as the 48-volt voltage source's initial interface (Figure 2).

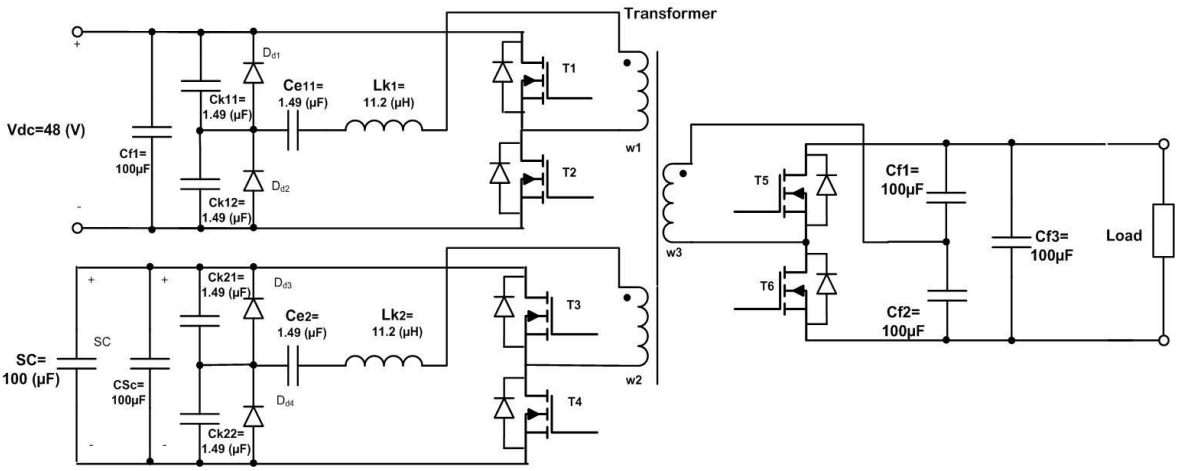

Figure 2. Schematic of a three-port converter with limiting diodes and values of components

The other part of the circuit has another port, port 2, which is known as the load port and functions as a signal driver by rectifying the DC voltage for the load connected to the end of the port. Port 3 is another component of the circuit known as the supercapacitor port, which handles bidirectional energy flow from the energy storage system. This part of the circuit transfers energy in two ways, acting as a half-bridge LLC circuit and a rectifier when the energy comes from a direct current source. This energy storage is achieved by

connecting 6 supercapacitor cells of 2 volts each in series to produce a voltage of 12 volts at the output. Similar to port 1, this port contains the LLC resonant circuit, which is connected with half-bridge transistors and then interfaced to the other ports using a 3 Winding electrical transformer. This high-frequency transformer with three windings serves for three basic functions: electrical isolation, magnetically combining input DC sources, and stepping up voltage from the low voltage side (LVS) to the high voltage side (HVS). The elements of energy transfer have a diversity that leaks inductance from them. This converter maintains a stable state by switching frequencies above the resonance frequency. MOSFET transistors are used to create switches, with Port 1 sending energy only in one direction and Port 3 enabling bidirectional current flow by charging and discharging the supercapacitor bank. The experimental setup depicted in Figure 3 is a laboratory-scale test designed to control and analyze the behavior of a three-stage resonant converter system using a computer-based interface. At the front end, a computer running LabVIEW is employed for signal generation, data acquisition, and control. It interfaces with a compact data acquisition device from National Instruments (DAQ-NI), which serves as a bridge between the digital commands and the physical circuits. Control signals are passed to optocoupler driver circuits (HCPL-3120) to ensure electrical isolation and safe signal transmission to the power stages. Each optocoupler driver is powered by a dedicated 15 Vdc external supply, enabling the safe switching of power devices across all stages of the converter (Figure 3).

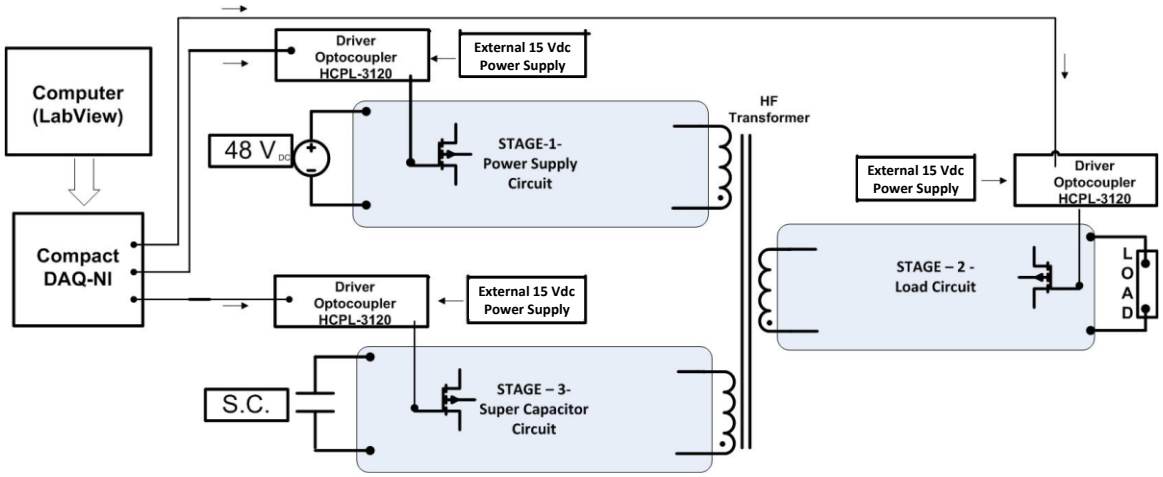

Figure 3. Block schematic of experimental setup and implementation

The three stages of the resonant converter are clearly visualized as: i) Stage 1 consists of a 48 V DC power supply feeding a resonant circuit through a driver-controlled switching mechanism; this section represents the main power input; ii) Stage 2 is the load circuit, which is connected via a High-Frequency Transformer to ensure galvanic isolation and voltage transformation between the stages; and iii) Stage 3 involves a supercapacitor circuit (S.C.), which functions as an energy storage buffer, providing support to the system during transient load demands or regenerative phases. The integration of LabVIEW, optocouplers, and individual stage controls enables fine-tuned real-time analysis and experimentation with power electronics behavior under different operating scenarios.

The experimental setup, illustrated in Figure 4, is the physical implementation of the schematic shown previously in Figure 3. It validates the operation of the proposed three-port resonant DC-DC converter under various load and source conditions. The system is controlled through a LabVIEW-based virtual instrument, which enables real-time monitoring and control. This interface is connected to a compact data acquisition unit (DAQ-NI) that provides digital output signals to the gate driver circuitry. These control signals are optically isolated using HCPL-3120 optocoupler drivers, enhancing electrical safety and ensuring accurate switching of the power semiconductors. As we can see, the converter is divided into three hardware stages circled with white color: Stage 1 corresponds to the input section connected to a DC power supply; Stage 2 forms the resonant circuit and switching interface, and the high-frequency transformer and rectifier block provides galvanic isolation and voltage conversion. The supercapacitor bank, connected as port 3, serves as the bidirectional energy storage element, and its voltage is monitored through a dedicated voltmeter. An external 15 Vdc power supply powers the gate driver circuitry.

At the output, a variable load resistor and a digital oscilloscope are used to evaluate output voltage and current waveforms. The voltage is also displayed for some stages using a digital multimeter. This setup enables controlled experimentation across all three operational modes, allowing comprehensive performance evaluation of energy transfer efficiency, switching behavior, and dynamic response of the converter. Figure 5 demonstrates experimentally successful energy transfer from the DC source to the load during mode 1 operation, in order to verify the simulation results. The top curve represents the load voltage, while the bottom curve displays the DC stage current of the resonant tank. The waveforms operate at a stable high frequency of 40 kHz, with a measured time interval (Δt) of 25.00 µs between key transition points, corresponding to the expected resonant behavior of the system. The clean, periodic waveforms with minimal distortion confirm efficient power transfer through the resonant tank and HF transformer, validating the theoretical design. In Figure 5, the DC offset of signal 2 is due to the use of a current probe. These results provide experimental confirmation of the converter's ability to maintain stable operation in mode 1 under the tested conditions.

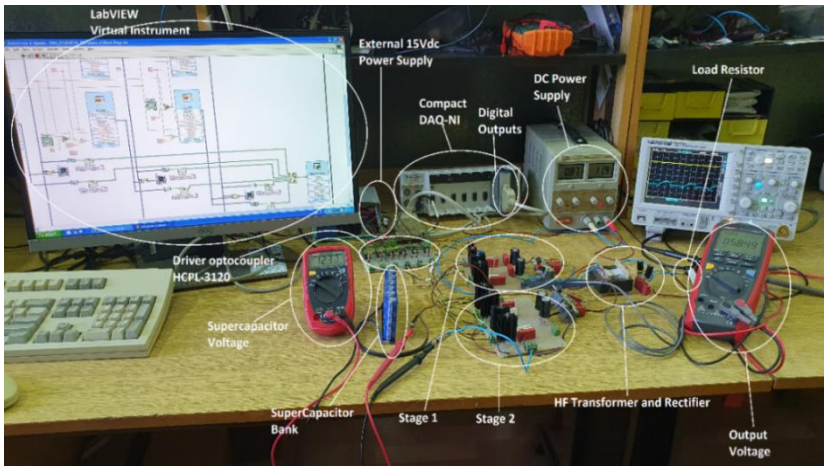

Figure 4. Block schematic of experimental setup and implementation

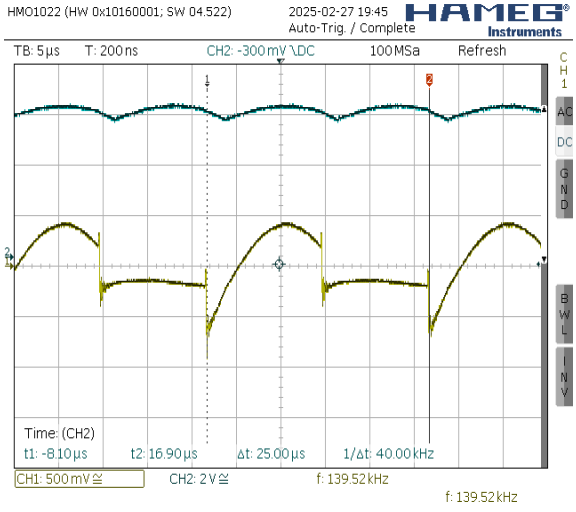

Figure 5. Block schematic of experimental setup and implementation

3. RESULTS AND DISCUSSION

The converter can be operated in three modes:

3.1. Mode 1 of operation: Energy transfer from the DC source to the load

This three-port DC-DC resonant converter system's performance depends on the transmission of energy from the DC power supply to the load. This part focuses on the possible modes of operation, particularly the behavior of currents and voltages in a DC power supply circuit. During Mode 1 of operation,

which represents the positive half-cycle of energy transfer from the DC source to the load, current follows the red-colored path indicated in the circuit diagram, Figure 6. Initially, the DC source energizes the resonant tank formed by capacitor Ce1 and inductor Lk1, initiating a resonant current flow. As switch T1 is turned ON through the control signals, the resonant current flows through the primary winding w1 of the high-frequency transformer Tr1. This excites the magnetic core, inducing a corresponding voltage on the secondary side. On the secondary, transistor T5 is synchronously switched to conduct, allowing the transferred energy to flow through it and into the output filter capacitor Cf2, which smooths the waveform before delivering it to the load. This cycle ensures high-frequency power transfer from the DC source to the load stage while minimizing switching losses thanks to resonant soft switching principles, and at the same time, stage 3 is not activated through the control system at all (Figure 6).

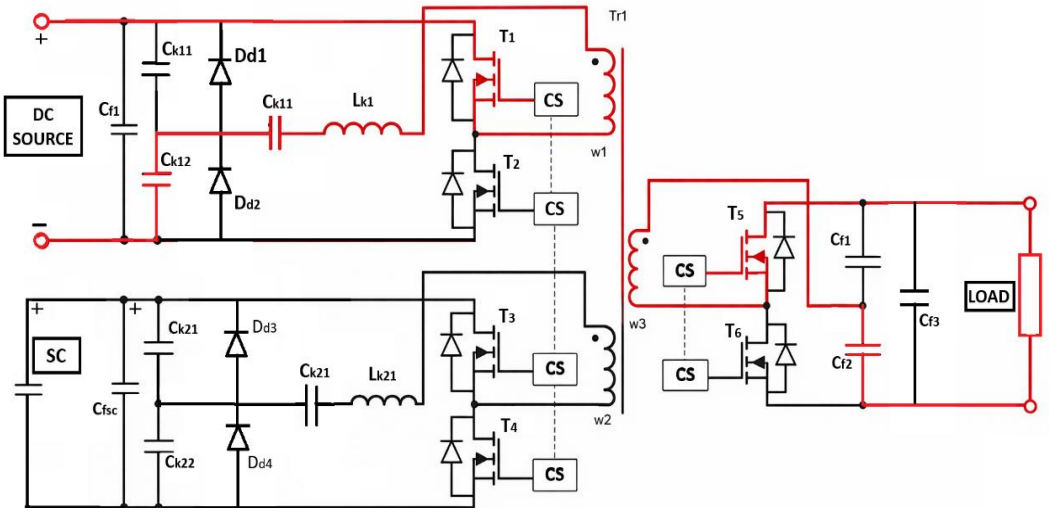

Figure 6. The positive half-cycle of energy transfer from the DC source to the load for Mode 1 of operation

Figure 7 illustrates the current and voltage waveform characteristics obtained during simulations for stage 1, DC power supply port. The DC power supply, which is the major energy source for the entire converter system, produces a constant voltage output, as illustrated in the figure. The red curve in Figure 7(a) depicts the voltage across the transistor simulated as FETD1 (T1), which serves as a controlled switch by turning on and off. Figure 7(b) shows the current flowing through the resonant tank, which has a near-sinusoidal waveform due to the LC resonance. This smooth alternating current confirms proper resonant operation and effective filtering of the high-frequency switching harmonics generated by T1. Figure 7(c) illustrates the resonant current within the resonant tank, which is synchronized with the operation of transistor T1 on the same port. Figure 7(d) shows the voltage across the transformer's Windings 1 and 2, which reflects the energy transfer process. Finally, the last graph in Figure 7(e), which is one of the most important components of this research, shows the output voltage transmitted from the DC source. It stabilizes at about 12 Vdc with a switching frequency of 111 kHz, which is much higher than the resonant frequency.

The current drawn from the DC power source fluctuates with the load requirements, as seen in Figure 8. This graph emphasizes the dynamic trend of the load current, demonstrating variations in the supply current as load demands alter over time. Transistor 1 (T1) plays a critical role in regulating energy flow from the power source to the converter, allowing the induced energy to pass through and be filtered by the output capacitor Cf2. The generated waveforms show that the current drawn from the power supply has half the switching frequency of transistor T1. This behavior occurs because the remaining current is conducted by the complementary transistor, transistor 2 (T2), within the pair. In this section of the study, we analyzed the operational modes of the "three-port DC-to-DC converter" system, namely the energy transfer from the DC power supply to the load. The steady-state output voltage sent from the power supply to the load resistance, together with transistor 1's regulated switching and the oscillatory dynamics of the resonant tank in the LLC circuit, provides the foundation for high-efficiency energy conversion.

3.2. Mode 2 of operation: Power transfer from the supercapacitor storage port to the load

The operational mode for transferring energy from the supercapacitor to the load involves a specific circuit arrangement that maximizes the use of the supercapacitor bank's stored energy. This section consists

more into the second mode of operation, focusing on the behavior of individual components and their influence on the circuit. During mode 2 of operation, the energy is transmitted from the supercapacitor (SC) to the load, representing the positive half-cycle or an auxiliary power delivery mode (Figure 9). The current path is highlighted in red in the provided diagram. In this mode, the supercapacitor bank discharges through the resonant tank formed by Ce2 and Lk2, initiating resonant oscillation. The driver-controlled switch T3 is turned ON, directing the resonant current through the primary winding w2 of the transformer Tr1, which then induces a corresponding voltage on the secondary side.

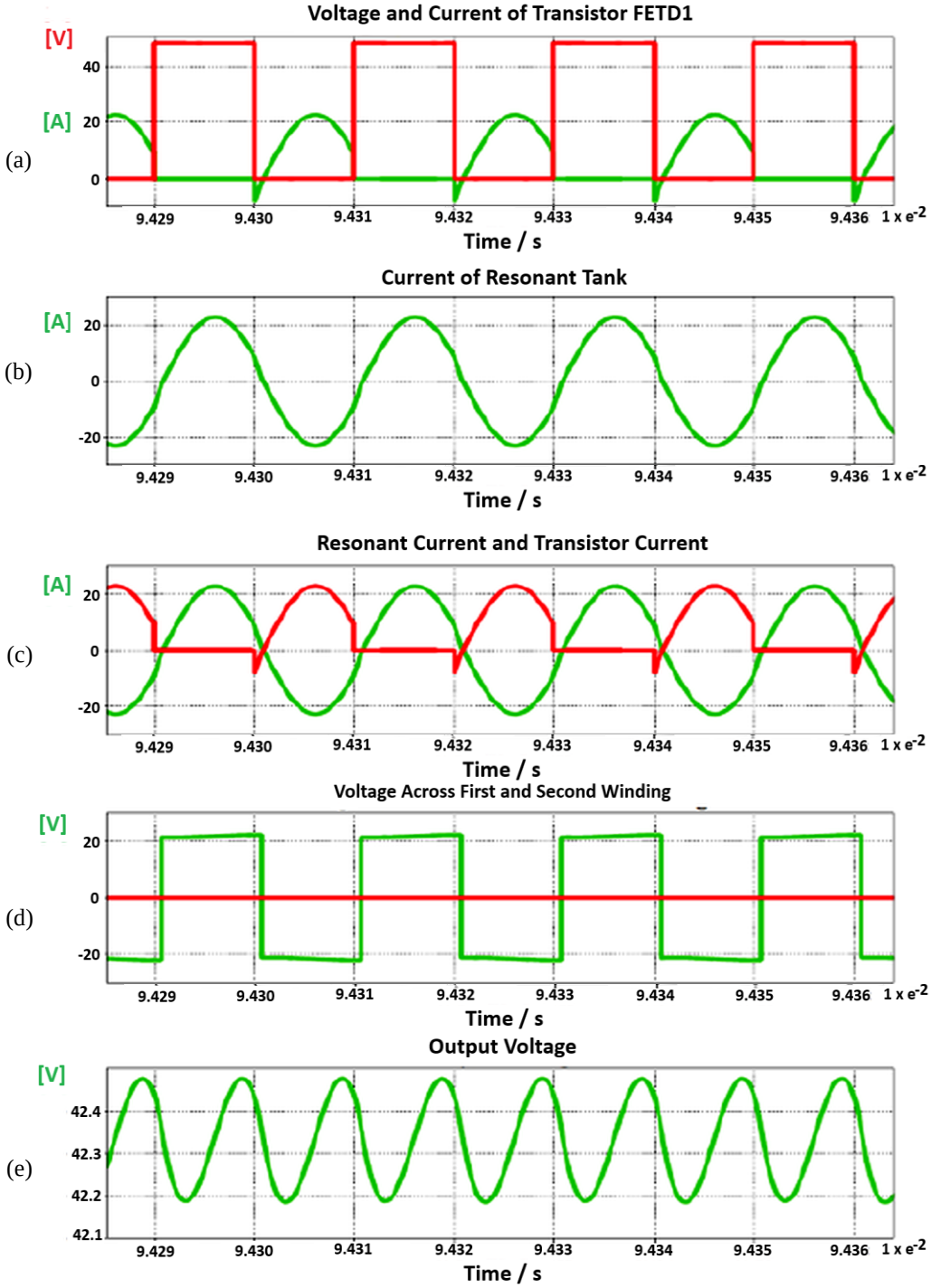

Figure 7. Simulated voltage and current waveforms of stage 1 (DC power supply port): (a) voltage across transistor T1 and its current, (b) resonant tank current, (c) resonant current and transistor current comparison, (d) voltage across the primary and secondary windings of the transformer, and (e) regulated output voltage waveform at 111 kHz switching frequency

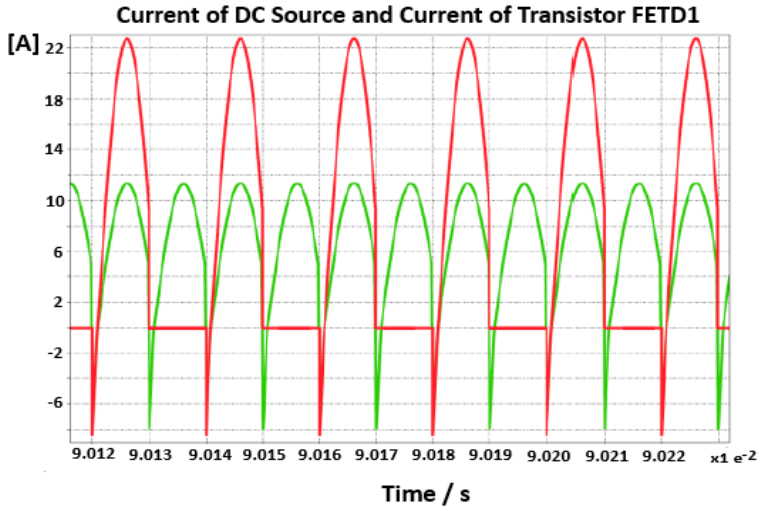

Figure 8. Current from the DC source and current through transistor 1

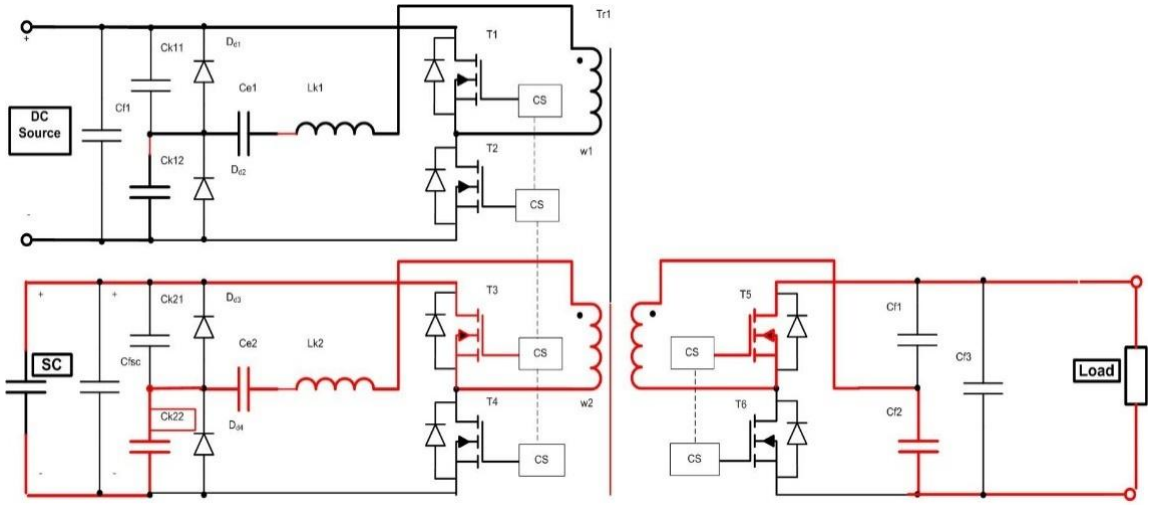

Figure 9. The positive half-cycle of energy transfer from the DC source to the load for mode 2 of operation

Simultaneously, the secondary switch T5 is activated, allowing the induced energy to pass through and be tunneled by the output capacitor Cf2. This ensures a smooth and continuous power flow to the load. Mode 2 is essential in applications requiring backup or auxiliary energy supply, utilizing stored energy in the supercapacitor to maintain power delivery without interruption, while also benefiting from soft-switching to reduce stress on switching devices. The interaction of these components is tuned in that way to ensure the energy is successfully transferred from the supercapacitor bank to the load while maintaining loyalty. This circuit has a pair of diodes known as limiting diodes, D3 and D4, whose purpose is to limit the amount of power that may be transferred from the storage bank to the load. When the resistive load is very low and close to a short circuit, these diodes will conduct a large current. When the resistive load reaches 5 Ohms, for example, at 20 or 50 Ohms these limiting diodes will not prevent electricity from the supercapacitor bank from reaching the load. Figure 10 shows the voltage and current measured at the load with a load resistance of 5 Ohms. This figure shows how the load behaves under various operating situations, with a focus on the voltage–current characteristics. The energy is stored in a supercapacitor bank made up of six completely charged supercapacitors, each with a maximum voltage of 2 V.

This energy is successfully transferred from the storage bank to the load via the resonant tank of port 3, the transformer, and the rectifier circuit on port 2. The energy flow travels through the circuits of ports 3 and 2, excluding the circuit of port 1. The block diagram illustrating the power transmission circuit is shown in Figure 10. Simulation studies were conducted with a supercapacitor voltage of USC = 16 V, a load

resistance of R Load = 10 Ω, and a switching frequency of 53 kHz. Figure 10(a) shows the current pulled from the supercapacitor bank, which corresponds to the voltage at the power bank's output. In this mode of operation, the energy drawn from the DC source is zero, as shown in Figure 10(b). This graph indicates that no energy is extracted from the DC source, as the current through the resonant tank (LK1) and transistor T1 (FETD1) both remain zero. Figures 10(c)-10(e) confirm that port 1 remains completely inactive during this mode of operation. The DC source current in Figure 10(c) is zero throughout the entire interval, indicating that no energy is extracted from the DC supply. Similarly, the resonant inductor current Lk1 is shown in Figure 10(d) remains zero, demonstrating that the resonant tank associated with port 1 is not engaged in the power transfer process. In addition, the transistor T1 current in Figure 10(e) is also zero, verifying that the switching device does not conduct. Together, these results confirm that energy transfer occurs exclusively between port 3 and port 2, while port 1 is electrically isolated in this operating mode.

Figure 11 displays the overall results for the current of transistor 1 and the current from the DC supply source. Figure 11(a) depicts the current through the resonant tank and limiting diode 1. The current through the resonant tank should have a nearly sinusoidal waveform, which is typical of a resonant circuit. Limiting Diode 1 will conduct when the voltage across it exceeds its forward voltage drop; otherwise, the current is zero. Analyzing this figure reveals information about the energy transmission between the resonant tank and the first limiting diode. Figure 11(b) depicts the current through limiting diode D3. The current through limiting diode 3 should be zero until the voltage across it hits the threshold. When the voltage surpasses this threshold, limiting diode D3 conducts, enabling current to flow in the opposite direction to the DC source and preventing overvoltage at the load. This diagram illustrates the point at which limiting diode D3 begins to conduct and the quantity of current it allows. Figure 11(c) depicts the resonant current and transistor current. The resonant current should oscillate as energy is passed between the resonant components, whereas the transistor current exhibits the transistor's switching capability by controlling the energy flow. Figure 11(d) depicts the current through limiting diode D4. This graph, similar to Figure11(b), gives information about the limiting diode D4 conduction characteristics. It indicates when the limiting diode D4 begins to conduct and the quantity of current it allows. These findings are based on the normal behavior of components in a resonant energy transfer system.

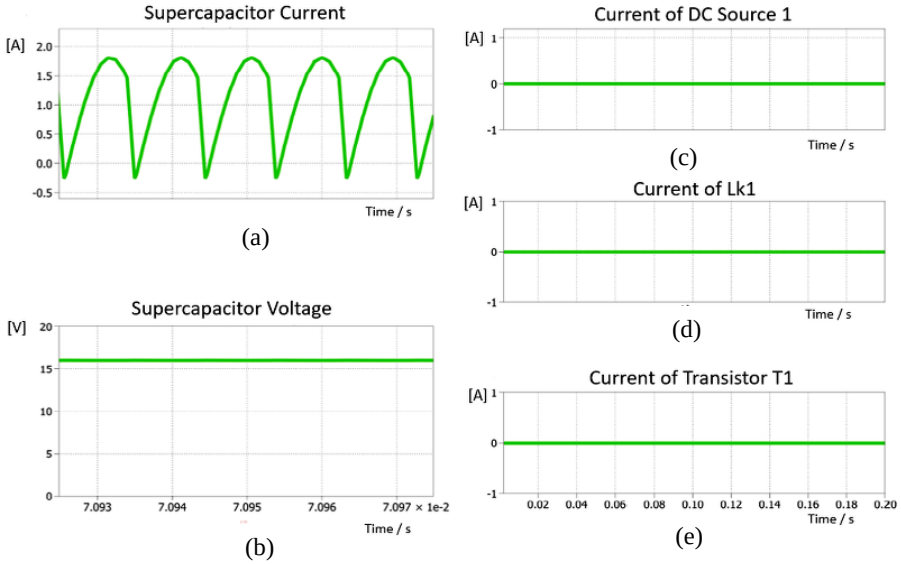

Figure 10. Power transfer from port 3 to port 2 under USC = 16 V, R_{load} = 10 Ω, and fs = 53 kHz: (a) supercapacitor current delivering energy to the load, (b) regulated supercapacitor voltage, (c) zero DC source current, (d) zero Lk1 current, and (e) zero T1 current, confirming that port 1 remains inactive during this mode

Figure 12 presents the key characteristics of the resonant LLC tank circuit for port 3, illustrating the energy flow from the supercapacitor bank to the load. The subfigures display more details for (a): transistor current and voltage. Figure 12(a) displays the current in the resonant inductor. The current in the resonant inductor should have a sinusoidal waveform, as in a resonant circuit.

Peaks in the current correlate to the points at which the inductor stores most of the energy. This waveform gives useful information on the energy transfer dynamics between the supercapacitor bank, the load, and the resonant tank. Figure 12(b) shows the current flowing through the transistor. The current flowing through the transistor should appear as a series of pulses or square waves, indicating its on-off switching characteristic. When the transistor is turned on, the current increases rapidly, signifying the energy transfer phase. When the transistor is turned off, the current drops to zero, indicating a break in energy transfer. Figure 12(c) in left down side illustrates the voltage across the transistor. The voltage across the transistor should follow a pattern consistent with its on-off switching. When the transistor is turned on, the voltage drop across it is minimal, suggesting effective conduction. When the transistor is turned off, the voltage increases due to the energy stored in the resonant tank seeking a discharge path. Monitoring this voltage is critical for determining the stress levels on the transistor and maintaining appropriate operation. Figure 12(d), upper right, depicts the steady-state voltage across the load, which approaches a constant value. This represents the voltage level that the load receives while in steady-state operation. Analyzing this figure offers information on voltage regulation and system stability. Figure 12(e) depicts the output current, which reaches a maximum of 1.2 A, indicating the maximum load current.

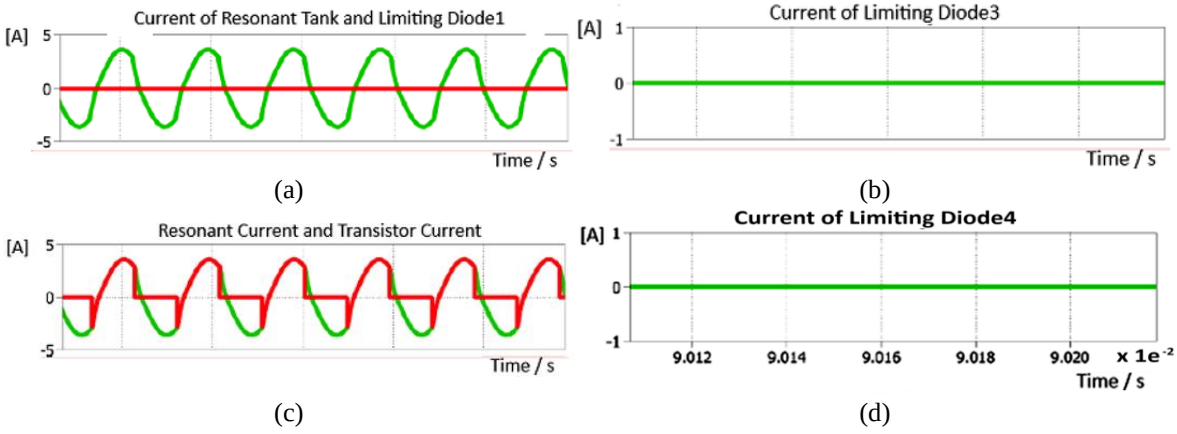

Figure 11. Stage 1 simulated current waveforms: (a) resonant tank and D1 currents, (b) D3 current, (c) resonant and T1 currents, and (d) D4 current during resonant operation

Mode 2 of the resonant energy transfer system, similar to Mode 1, enables controlled power delivery from the supercapacitor storage bank to the load while maintaining a regulated 12 V DC output. In this mode, the resonant LLC tank in Port 3 shapes the energy transfer by producing a near-sinusoidal resonant inductor current, which supports efficient high-frequency power transmission. The limiting diodes provide a current path only when their forward-bias condition is satisfied, which helps prevent reverse energy flow and protects the circuit against abnormal voltage conditions. At the same time, the transistor operates as the main switching element that controls when energy is injected into the resonant network, defining the conduction intervals and the delivered power level. As a result, the converter achieves stable output operation with reduced switching stress and improved overall reliability during the supercapacitor-to-load transfer process.

3.3. Mode 3 of operation: Simultaneous energy transfer from the DC power supply and power bank to the load

In this section, we analyze this three-port DC-DC converter operational dynamics, with a focus on the third mode of operation. This mode demonstrates the converter's capability to efficiently transfer energy across several ports: the DC power source (port 1), the load (port 2), and the supercapacitor (port 3). In Mode 3 of operation, energy is simultaneously delivered from both the DC power supply and the supercapacitor storage bank to the load, enhancing the overall power capacity and improving transient response. This hybrid mode is crucial during high load demands or startup conditions. As shown in the diagram, both the upper and lower converter stages operate in parallel. The DC source drives current in positive half cycles, as shown in red line directions in Figure 12, through the resonant components Ce1 and Lk1, while the supercapacitor discharges through its respective resonant path consisting of Ce2 and Lk2. Power switches T1, T3, and T5 are appropriately controlled to synchronize the primary side operation of both inputs, energizing transformer windings w1 and w2 simultaneously. On the secondary side, switches T5 and T6 (for both cycles) coordinate

the combined energy transfer to the load, while output filter capacitors Cf1, Cf2, and Cf3 smooth the resulting voltage. This collaborative energy sharing not only reduces stress on a single source but also enhances reliability and system efficiency by intelligently utilizing both energy reservoirs (Figure 13).

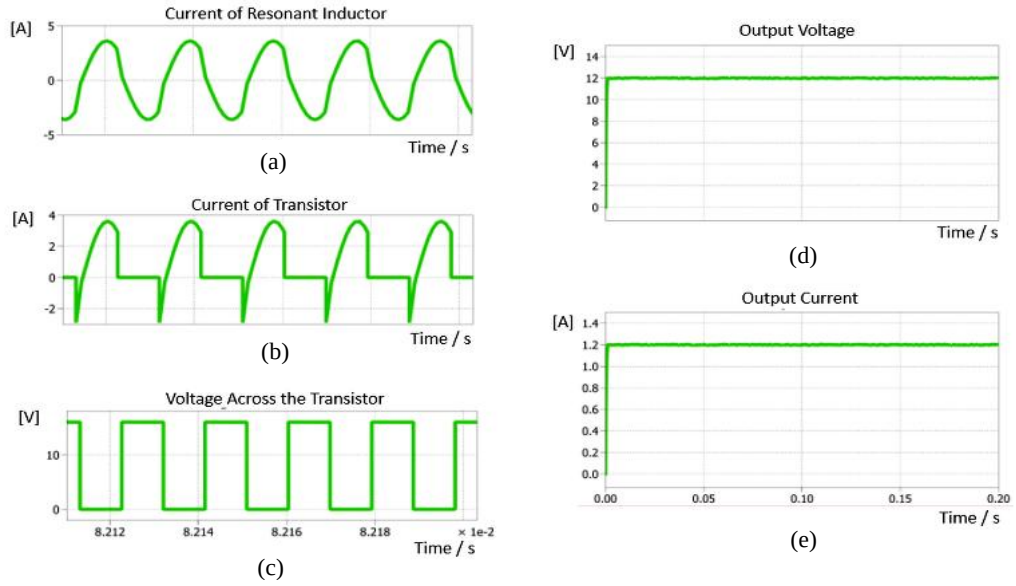

Figure 12. Simulated characteristics of the port 3 resonant LLC tank during energy transfer from the supercapacitor bank to the load: (a) resonant inductor current waveform, (b) transistor current waveform, (c) voltage across the transistor during switching, (d) regulated output voltage response, and (e) output current delivered to the load

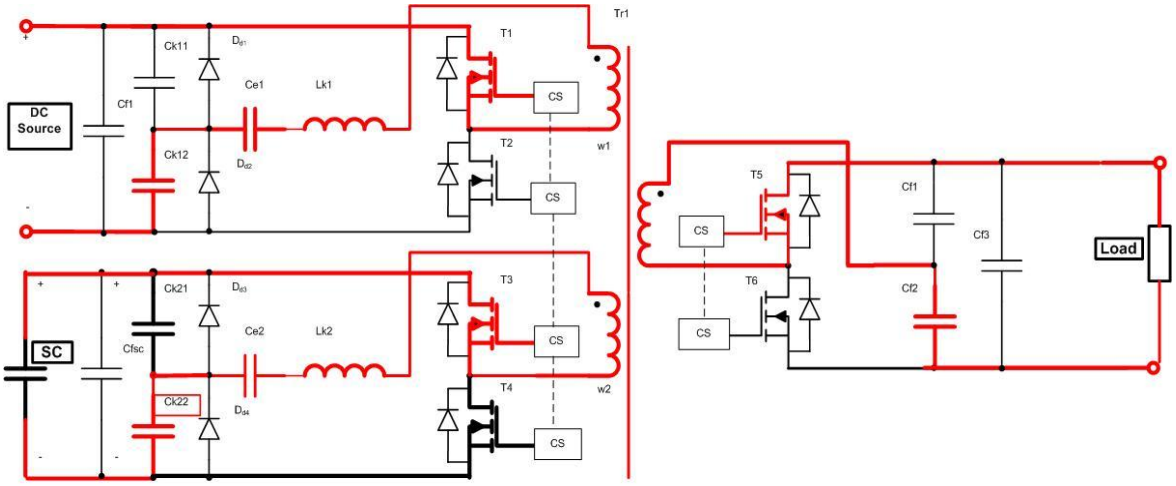

Figure 13. The positive half-cycle of energy transfer from the DC source to the load for Mode 3 of operation

Based on the simulation findings, it was found that in order to maintain a constant output voltage of 12 V, the control system must first measure the load value to determine an acceptable switching frequency for various resistances. This mode is especially useful in situations where energy must be efficiently transferred between these ports, such as hybrid energy systems for residential as well as electric vehicles. Figure 14 shows extensive information regarding the behavior of several components in the circuit built for Mode 3 operation. It enables detailed examination of transistor behavior, load performance, power supply characteristics, and control signal efficiency.

Figure 14(a) displays the current and voltage of Transistor T1. This graph shows the transistor's current-voltage characteristics, which are critical for understanding the behavior of DC-DC converters in the

circuit. The graph aids in analyzing the transistor's performance and ensuring it works within safe limits. The voltage and current are synchronized at the beginning and end points of each period. Figure 14(b) depicts the voltage and current of transistor T1 in Mode 3 of operation, which maintains around 12 V. This confirms that the output voltage remains consistent across all modes of operation. Figure 14(c) shows the output voltage across the load. This section of the diagram depicts the voltage applied to the load, which is the component that the circuit is intended to power (such as a motor, light bulb, or other electrical components). Monitoring the output voltage is critical to ensuring that the load receives the appropriate amount of power and that the circuit operates properly. Figure 14(d) most likely depicts the behavior of the DC power supply that powers the circuit. This graph could show the current provided by the power supply over time. Optimizing the power supply behavior under various scenarios is critical for ensuring dependable operation and preventing overload. Figure 14(e) depicts the pulse generator signals that drive the transistors. These signals, usually in the form of pulses, control when the transistors switch on and off. With a load resistance of 1 Ω, the frequency falls below the resonance frequency of 42 kHz. The timing, duration, and frequency of these pulses are important for effectively driving the transistors to achieve the desired performance.

Figure 15 depicts the dynamic behavior of the supercapacitor's current and voltage while operating in this mode. The graph depicts the current waveform drawn from the battery, emphasizing the energy transfer mechanism in the system. At the same time, the voltage between the battery terminals remains constant at 12 Volts, indicating the system's reliability in DC output.

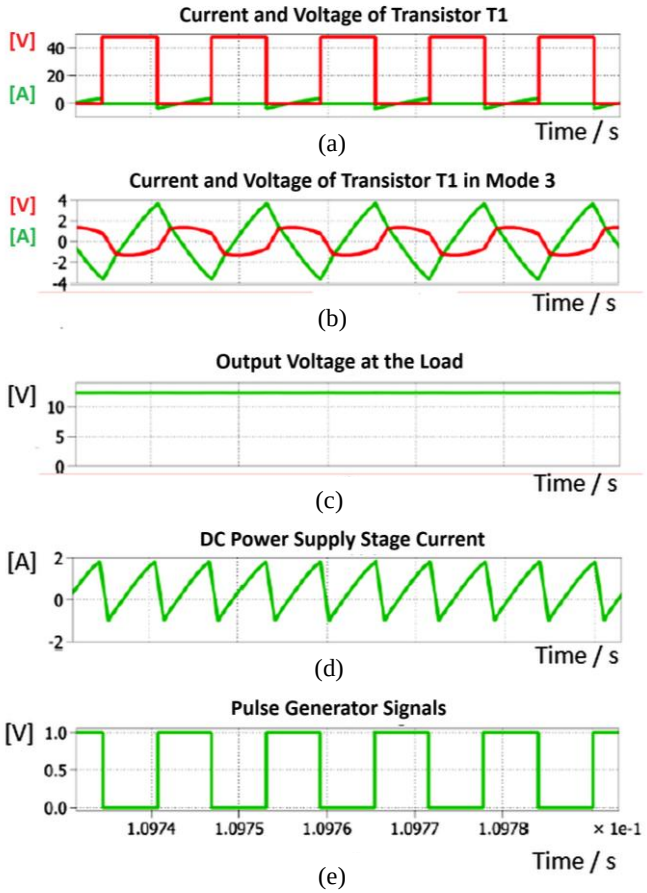

Figure 14. Simulated waveforms in Mode 3 of operation under R_{load} = 1 Ω and switching frequency below the resonant frequency (42 kHz): (a) voltage and current of transistor T1 illustrating its switching behavior and synchronized turn-on and turn-off transitions, (b) transistor T1 voltage and current confirming regulated 12 V operation, (c) output voltage across the load, (d) DC power supply current response during operation, and (e) pulse generator gate signals controlling the transistor switching sequence

The current waveform follows a cyclical pattern, which is typical for resonant energy systems. Peaks in the current correlate to moments when the system pulls the most power from the battery, whilst it

represents periods of low energy use. This rhythmic motion demonstrates the battery's efficient use of stored energy. The stable 12 V output voltage demonstrates the system's capacity to produce consistent power and satisfy the load demands without risking the stability of operation. Figure 16 shows a detailed depiction of the system's dynamic currents, emphasizing the interaction between the DC source, inductor Lk1, and transistor T1. The dominant waveform in Figure 16(a) depicts the cyclical current obtained from the DC source. This current profile shows the system's energy demand over time, with frequent peaks and troughs. Peaks in the cycle current waveform indicate when the system takes the most power from the DC source to fulfill the load needs, while represent periods of low energy consumption, displaying the system's power management. Figure 16(b) shows the current flowing through inductor Lk1, which is a basic element for the resonant tank of stage 1.

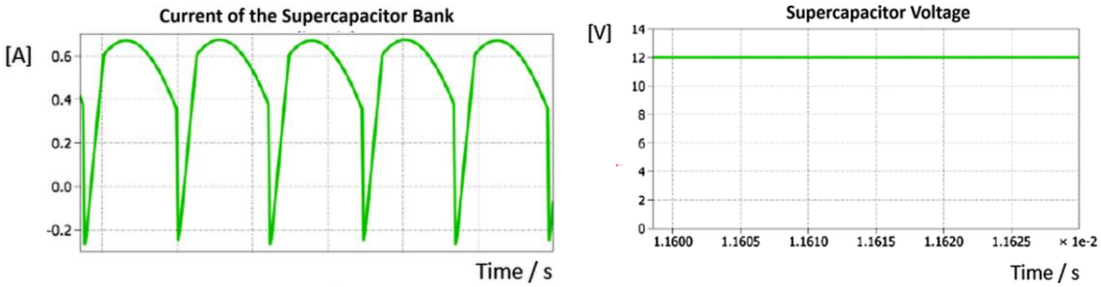

(a) (b)

Figure 15. Dynamic response of the supercapacitor during operation: (a) supercapacitor bank current waveform showing the periodic discharge behavior and energy transfer to the load, and (b) supercapacitor terminal voltage remaining regulated at 12 V, confirming stable DC output performance

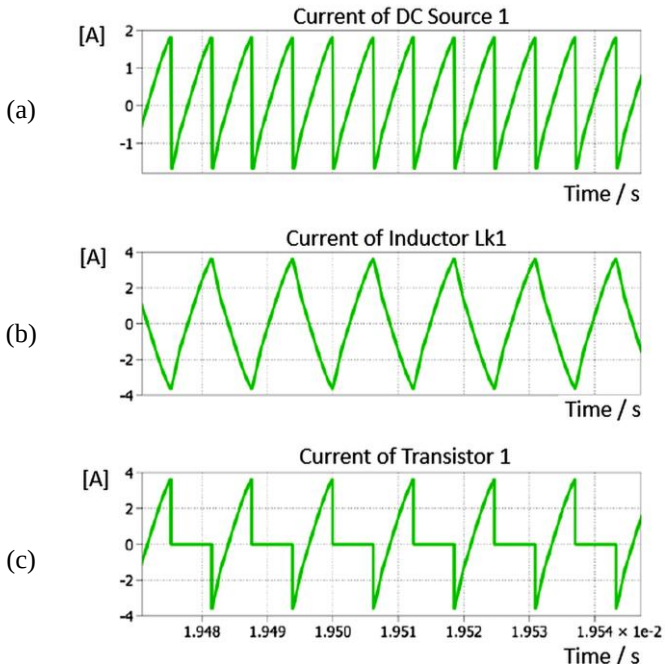

Figure 16. Simulated current waveforms illustrating the dynamic interaction between the DC source and resonant stage: (a) DC source current showing periodic energy extraction, (b) resonant inductor Lk1 current exhibiting oscillatory behavior characteristic of the resonant tank, and (c) transistor T1 (FETD1) current indicating controlled switching intervals and regulated energy transfer

The half-wave signal current from transistor T1 in Figure 16(c), complements the other waveforms. This current shows the transistor switching behavior, which is important for managing energy flow. The half-wave signal current has distinct on-off cycles, suggesting that transistor T1 switches between conducting and

non-conducting states. When the transistor conducts, the current rapidly increases, allowing energy to be transferred from the DC source to the load. During non-conducting phases, the current drops to zero, indicating a stop in energy transmission and effective power management. The dynamic currents displayed in Figure 16 work together to provide a thorough understanding of the system energy dynamics. They demonstrate the cyclical nature of energy consumption from the DC source, the resonant energy exchange in inductor Lk1, and the exact regulation of energy flow via transistor T1.

4. DISCUSSION

This paper analyzes a novel DC/DC converter technique for energy storage systems in renewable energy applications. The findings indicate that, while these converters are efficient, their operation needs a more complex control system. To create a clear comparative framework with the latest research, Table 1 provides a systematic evaluation of five modern DC-DC converter topologies (multi-port DC, boost multiport interleaved step-up, isolated bidirectional, voltage/current FED, and general resonant) based on seven key performance parameters. Using validated data from peer-reviewed sources, including the review in [47], the analysis highlights key differences, for example, the general resonant converter achieves high efficiency (96%) with fewer components, while the multi-port DC offers strong soft-switching (ZVS/ZCS) performance but involves more complexity and higher cost.

Table 1. Systematic evaluation of five modern DC-DC converter topologies

Comparison criteria	Multi-port DC converters - presented converter	Boost multiport interleaved StepUp [47]	Isolated bidirectional [47]	Voltage and current [47]	General resonant [47]
Component numbers	– Active transistors: 6 – Passive L: 3, C: 9, Tr. 1,	– Active transistors: 2 – Passive L: 2, C: 2, Tr. 0,	– Active transistors: 4, 8 – Passive L: 1, 1 C: 2, 2 Tr. 1, 1	-Active Transistors: 4, 4 -Passive L: 1, 1 C: 2,12 Tr. 1, 1	-Active Transistors: 4 -Passive L: 1 C: 2 Tr. 1
Voltage stresses	– V (Input): – SC voltage – V out	$\frac{1-2D}{1-D}$ x Vout	(1 - D)×Vout	$\frac{1-D}{D}$ ×Vout	(1-D)×Vout
Current stress	– Resonant current – ZVS – ZCS	Low current stress	Medium current stress	Low current stress	Low current stress
Complexity	– High complex – 2 Resonant stages – Possibility to drive under resonant frequency – Above Resonant freq. – Independent between the legs	Medium complexity	High complexity	Medium complexity	Low complexity
Total cost	High ($120)	Medium ($80)	High ($110)	Medium ($90)	Low ($70)
Efficiency	High efficiency expected (96%)	95%	93%	94%	96%
Control system	– Complex (Digital) – Driving transistors with different frequencies	Medium (Analog)	Complex (Digital)	Medium (Analog)	Simple (PWM)

The comparison highlights fundamental engineering trade-offs: simpler topologies like the General Resonant converter favor cost-effectiveness and ease of control (PWM), making them ideal for commercial applications, while complex designs like the multi-port DC converter enable specialized functions (bidirectional power flow) for demanding environments like renewable energy systems. Efficiency metrics and current stress levels further differentiate suitability for high-power vs. precision applications. This structured analysis enables informed topology selection based on specific project requirements for power electronics design.

Table 2 presents a targeted comparative analysis of two advanced DC-DC converter topologies: multiport DC with limiting diodes and general resonant converters, highlighting their respective advantages, limitations, and application domains to guide technology selection in power electronics design. The multiport DC topology demonstrates superior power density and bidirectional capability enabled by soft switching

(ZVS/ZCS), although with higher complexity (sensitive control systems) and cost from resonant components. It is ideal for renewable energy integration (PV/wind hybrids, EV charging) and microgrid applications. In contrast, the General Resonant converter achieves peak efficiency with simpler PWM control and low EMI generation, though constrained by limited voltage gain and poor light-load regulation. These features make them ideal for precision applications such as data centers, aerospace systems, and medical power supplies, where high efficiency is more important than a wide dynamic range. This structured comparison, grounded in IEEE-reviewed metrics [47]-[50] and complementary research, crystallizes critical trade-offs often overlooked in isolated topology studies, thereby offering engineers a consolidated structure for application. Table 1 summarizes and compares five representative DC-DC converter structures with respect to active and passive component requirements, voltage stress relations, current stress performance, and implementation complexity, providing a structured overview of their design trade-offs. Table 2 compares the multiport DC converter with limiting diodes and the general resonant converter in terms of key advantages, disadvantages, and typical application areas, highlighting their operational strengths and practical trade-offs.

Table 2. Comparative analysis of two advanced DC-DC converter topologies

Evaluation criteria	Advantage	Disadvantage	Apricate application
1. Multiport DC with limiting diodes	– High power density – Soft-switching capability (ZVS/ZCS) – Bidirectional power flow –	– Complex control system – Higher cost due to resonant components – Sensitivity to parameter variations	– Renewable energy systems – (PV/wind hybrid systems) – EV fast charging stations – Microgrid interconnections
2. General resonant	– Highest efficiency (96%) – Simple PWM control – Low current stress – Low EMI generation	– Limited voltage gain range – Requires precise resonant tuning – Poor regulation at light loads	– High-efficiency DC-DC conversion (data centers, telecom) – Aerospace power systems – Medical power supplies

In our case study, we simulated the system at lower resistance values, such as 1 and 5 Ohms (near to short circuit circumstances), and subsequently extended the simulations to larger resistances up to 100 Ω. In this study, we discovered that in order to maintain a consistent output voltage of 12 V across all three modes of operation, the converter's switching frequency must be changed for each change in load resistance. As a result, before the converter enters a specific mode with a given resistance, an algorithm for measuring the resistance must be developed. The control system is then configured with the converter's operating frequency. This method must be completed in 26 microseconds to verify that the output voltage meets the target value for each resistance and operating frequency. This is one of the downsides of the resonant converter, as it needs a more complex control system, despite its superior performance and efficiency over other topologies.

During the development and testing of the proposed three-port resonant DC-DC converter, several technical challenges were encountered that influenced the design decisions and overall system performance. These include: i) Current limitation via protection diodes: Each mode of operation incorporates current-limiting diodes to safeguard the circuit components against overload conditions. These diodes are particularly active in Modes 1 and 2, which involve energy transfer from the DC source to the load and to the supercapacitor, respectively. While they enhance protection, they also impose constraints on maximum current flow, potentially limiting power transfer capability under heavy loads; ii) Wide range of changes in driving frequency: To achieve precise output voltage regulation, the converter's switching frequency must be adjusted across a wide range. This broad frequency variation introduces electromagnetic noise with wide spectral characteristics, challenging the electromagnetic compatibility (EMC) of the entire system. Additional filtering or shielding may be required to comply with EMC standards in real-world applications; iii) Voltage matching between supercapacitor and DC Source: Efficient operation in Mode 2 (charging the supercapacitor) requires a carefully selected voltage range for the supercapacitor relative to the DC source. A poorly matched voltage range complicates bidirectional energy flow, requiring complex control logic to stabilize transitions between modes; iv) Capacitive output behavior and soft output characteristics: The load port exhibits a capacitive output nature, meaning the output voltage is highly sensitive to changes in current demand. This results in a “soft” output characteristic where even small variations in load current cause noticeable voltage fluctuations, requiring precise control and filtering to maintain output stability; v) Tight resonant tank matching between ports: The resonant tanks associated with the DC source and the supercapacitor must have nearly identical electrical characteristics. Any significant mismatch, such as differing inductance or capacitance values, can lead to unbalanced operation and instability, particularly in Mode 3 where both energy sources contribute simultaneously; vi) Impact of load stage to capacitance on resonance: If the output-stage capacitors (connected at the load) are small or similar in value to the resonant capacitors, they significantly alter the overall resonance behavior of the circuit. This unintended interaction

can shift the resonance frequency and degrade performance, making careful selection of output capacitance critical; and vii) Transformer turn ratio constraints: The transformer windings across all three ports must maintain similar turn ratios. A large deviation between these ratios disrupts the predefined operating modes and results in imbalanced power transfer. Consistent turn ratios ensure synchronized resonance and proper power sharing across all ports.

Figure 17(a) illustrates how the DC output voltage varies with load resistance at a short circuit (1 Ω), as well as the current through transistor 1 and Mode 1 output voltage, which maintains around 12 Vdc. The switching frequency in this example is 48 kHz. In Figure 17(b), the load resistance is 1 Ω, with a switching frequency of 42 kHz. Figure 17(c) replicates a load resistance of 10 Ω in Mode 1 at 111 kHz. In Figure 17(d) simulates a 10 Ω load resistance in Mode 3 at a switching frequency of 101 kHz. These findings emphasize the significance of load resistance in shaping the output voltage behavior. Impact of Load Resistance: Higher load resistance has been shown to result in decreased current draw, which aids in the stabilization of the output voltage. This is especially relevant for applications that require continuous voltage levels. Considerations for frequency: The changes in frequency between modes highlight the relevance of the circuit's operating frequency. Aside from load resistance, problems associated with higher frequencies, such as switching losses and transient reactions, can have an impact on performance.

Transistor operation: The performance of transistor 1 under various load and frequency settings sheds light on its efficiency and operating constraints. Understanding how these elements interact is essential for optimizing circuit design in power electronics. Finally, this paper emphasizes the importance of both resistance levels and operating frequencies in electronic circuit design, demonstrating the relationship between load resistance and DC output voltage using practical examples.

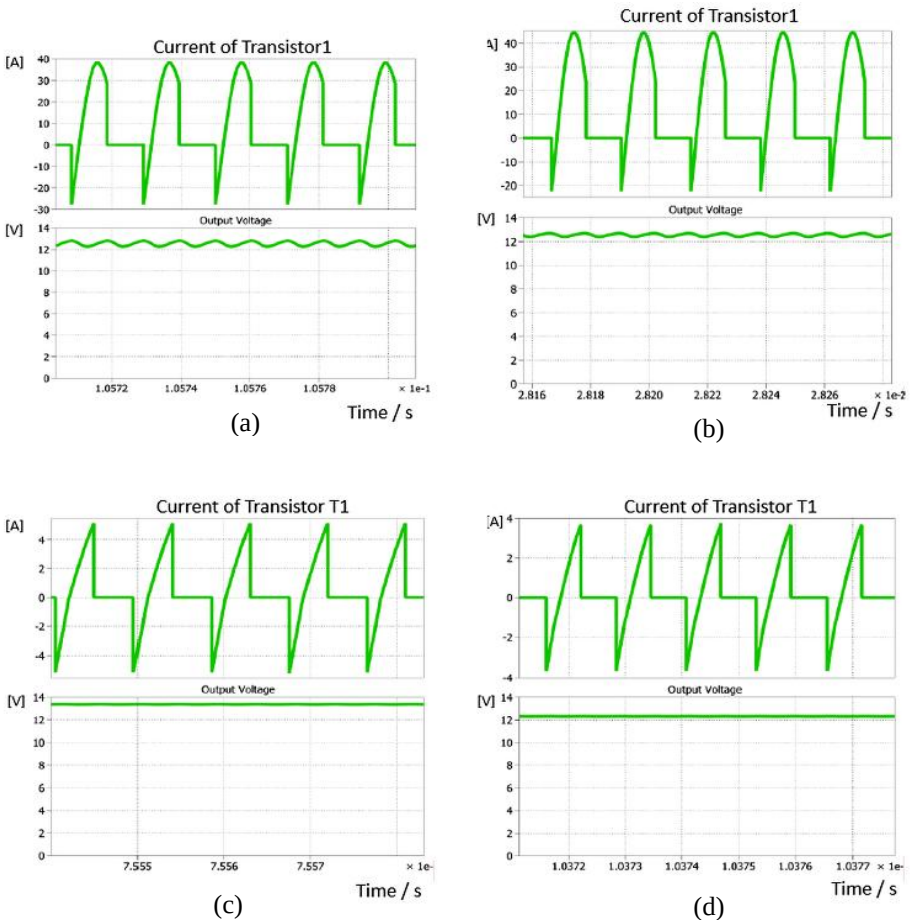

Figure 17. Dependence of the DC output voltage on load resistance: (a) Current of Transistor 1 and output voltage for Mode 1 with a 1-ohm load (frequency 48 kHz); (b) Current of Transistor 1 and output voltage for Mode 3 with a 1-ohm load (frequency 42 kHz); (c) Current of Transistor 1 and output voltage for Mode 1 with a 10-ohm load (frequency 111 kHz); and (d) Current of Transistor 1 and output voltage for Mode 3 with a 10-ohm load (frequency 101 kHz)

5. CONCLUSION

In this paper, the three-port DC-DC converter with energy storage, specifically designed for renewable energy systems, is analyzed. The unique design of the converter enables efficient energy transfer from multiple sources to the load, improving overall energy management and utilization. Through the analysis of three distinct modes of operation, we have gained valuable insights into the capabilities and performance characteristics of the converter.

Mode 1: Energy transfer from the DC source to the load

In Mode 1, the converter efficiently transfers energy from the DC power source to the load. The analysis of this mode has demonstrated the system's ability to provide a stable voltage output to the load while accommodating varying load demands. The converter's capability to control both output voltage and current makes it highly suitable for applications in renewable energy systems, ensuring reliable power delivery to the load.

Mode 2: Energy transfer from the power bank to the load.

Mode 2 focuses on transferring energy from the power bank to the load. Through in-depth analysis, we observed the dynamic interaction between the supercapacitor bank, the resonant tank circuit, and key control components such as transistors and limiting diodes. The current profiles generated in this mode exhibit sinusoidal behavior, reflecting the resonant energy exchange within the system. This mode ensures that stored energy in the power bank is efficiently utilized to supply power to the load, enhancing the overall system's efficiency.

Mode 3: Energy transfer from DC source and supercapacitor to the load

In Mode 3, both the DC source and the supercapacitor work together to supply energy to the load. This mode is activated when additional power is required, ensuring a stable and efficient energy transfer. The supercapacitor helps manage transient loads, reducing strain on the DC source and improving system reliability. Proper synchronization of the resonant converters is crucial to balance power distribution and prevent inefficiencies. Simulation studies at different voltage levels, such as 24 V and 36 V, confirm the effectiveness of this mode in enhancing performance and maintaining a steady power supply.

6. OVERALL PERFORMANCE AND CONTRIBUTIONS

Through simulation studies and analysis of the three operational modes, we have established the converter's efficiency, stability, and adaptability in renewable energy applications. The converter's ability to regulate voltage, manage varying load demands, and facilitate seamless energy transfer from different sources underscores its significance in modern renewable energy systems. The findings presented in this paper contribute to the advancement of a three-isolated-port DC/DC converter with energy storage, providing a framework for efficient power management in renewable energy applications. Future work may focus on experimental validation of the proposed converter, further optimization of control strategies, and integration into real-world renewable energy systems. With continued research and development, converters of this nature hold promise for enhancing the reliability, efficiency, and sustainability of renewable energy infrastructure. In conclusion, a three-isolated-port DC/DC converter with energy storage, as explored in this study, stands as a promising solution for addressing the evolving needs of renewable energy systems, paving the way for a more resilient and sustainable energy future.

ACKOWLEDGEMENT

This research is carried out within the framework of the project "Optimal work of power electronic converters in hydrogen technology – Hydrogen-to-X applications," КП-06-Н87/10 06.12.2024, Bulgarian National Scientific Fund. All simulations in this paper were carried out using PLECS software from PLEXIM under the PLECS Academic Sponsorship agreement between the Technical University of Sofia and PLEXIM GmbH.

FUNDING INFORMATION

This publication fee was funded by Bulgarian National Scientific Fund within the framework of the project "Optimal work of power electronic converters in hydrogen technology – Hydrogen-to-X applications," КП-06-Н87/10 06.12.2024.

AUTHOR CONTRIBUTIONS STATEMENT

This journal uses the Contributor Roles Taxonomy (CRediT) to recognize individual author contributions, reduce authorship disputes, and facilitate collaboration.

Name of Author	C	M	So	Va	Fo	I	R	D	O	E	Vi	Su	P	Fu
Faruk Ahmeti	✓	✓	✓	✓	✓	✓		✓	✓	✓		✓	✓	✓
Dimitar Arnaudov	✓	✓	✓		✓	✓	✓	✓	✓	✓	✓	✓	✓	✓
Sabrije Osmanaj	✓				✓	✓		✓	✓	✓	✓	✓	✓	✓

C : **C**onceptualization
M : **M**ethodology
So : **So**ftware
Va : **Va**lidation
Fo : **Fo**rmal analysis
I : **I**nvestigation
R : **R**esources
D : **D**ata Curation
O : Writing - **O**riginal Draft
E : Writing - Review & **E**diting
Vi : **Vi**sualization
Su : **Su**pervision
P : **P**roject administration
Fu : **Fu**nding acquisition

CONFLICT OF INTEREST STATEMENT

The authors state there is no conflict of interest.

DATA AVAILABILITY

The authors confirm that the data supporting the findings of this study are available within the article.

REFERENCES

[1] F. Wu, X. Li, F. Feng, and H. B. Gooi, "Multi-topology-mode grid-connected inverter to improve comprehensive performance of renewable energy source generation system," *IEEE Transactions on Power Electronics*, vol. 32, no. 5, pp. 3623–3633, 2017, doi: 10.1109/TPEL.2016.2589974.

[2] F. Blaabjerg and K. Ma, "Future on power electronics for wind turbine systems," *IEEE Journal of Emerging and Selected Topics in Power Electronics*, vol. 1, no. 3, pp. 139–152, 2013, doi: 10.1109/JESTPE.2013.2275978.

[3] H. Wu, Y. Xing, Y. Xia, and K. Sun, "A family of non-isolated three-port converters for stand-alone renewable power system," in *IECON Proceedings (Industrial Electronics Conference)*, IEEE, 2011, pp. 1030–1035. doi: 10.1109/IECON.2011.6119337.

[4] K. Sun, L. Zhang, Y. Xing, and J. M. Guerrero, "A distributed control strategy based on DC bus signalling for modular photovoltaic generation systems with battery energy storage," *IEEE Transactions on Power Electronics*, vol. 26, no. 10, pp. 3032–3045, 2011, doi: 10.1109/TPEL.2011.2127488.

[5] F. Locment, M. Sechilariu, and I. Houssamo, "DC load and batteries control limitations for photovoltaic systems. experimental validation," *IEEE Transactions on Power Electronics*, vol. 27, no. 9, pp. 4030–4038, 2012, doi: 10.1109/TPEL.2012.2189134.

[6] F. Ahmeti, S. Osmanaj, and D. Arnaudov, "Comparative analysis and optimization parallel operation strategies in dc-dc converters for smart dc grid integration," in *2024 International Conference on Renewable Energies and Smart Technologies, REST 2024*, IEEE, 2024. doi: 10.1109/REST59987.2024.10645476.

[7] Z. Rehman, I. Al-Bahadly, and S. Mukhopadhyay, "Multiinput dc-dc converters in renewable energy applications - an overview," *Renewable and Sustainable Energy Reviews*, vol. 41, pp. 521–539, 2015, doi: 10.1016/j.rser.2014.08.033.

[8] R. Faraji, H. Farzanehfard, G. Kampitsis, M. Mattavelli, E. Matioli, and M. Esteki, "Fully soft-switched high step-up non-isolated three-port DC-DC converter using gan hemts," *IEEE Transactions on Industrial Electronics*, vol. 67, no. 10, pp. 8371–8380, 2020, doi: 10.1109/TIE.2019.2944068.

[9] J. Hong, J. Yin, Y. Liu, J. Peng, and H. Jiang, "Energy management and control strategy of photovoltaic/battery hybrid distributed power generation systems with an integrated three-port power converter," *IEEE Access*, vol. 7, pp. 82838–82847, 2019, doi: 10.1109/ACCESS.2019.2923458.

[10] Z. Wang, Q. Luo, Y. Wei, D. Mou, X. Lu, and P. Sun, "Topology analysis and review of three-port DC-DC converters," *IEEE Transactions on Power Electronics*, vol. 35, no. 11, pp. 11783–11800, 2020, doi: 10.1109/TPEL.2020.2985287.

[11] H. Wu, K. Sun, S. Ding, and Y. Xing, "Topology derivation of no isolated three-port DC-DC converters from DIC and DOC," *IEEE Transactions on Power Electronics*, vol. 28, no. 7, pp. 3297–3307, 2013, doi: 10.1109/TPEL.2012.2221746.

[12] H. Wu, Y. Xing, Y. Xia, and K. Sun, "A family of non-isolated three-port converters for stand-alone renewable power system," *IECON Proceedings (Industrial Electronics Conference)*, pp. 1030–1035, 2011, doi: 10.1109/IECON.2011.6119337.

[13] S. Ding, H. Wu, Y. Xing, Y. Fang, and X. Ma, "Topology and control of a family of non-isolated three-port DC-DC converters with a bidirectional cell," in *Conference Proceedings - IEEE Applied Power Electronics Conference and Exposition - APEC*, IEEE, 2013, pp. 1089–1094. doi: 10.1109/APEC.2013.6520435.

[14] Y. Chen, G. Wen, L. Peng, Y. Kang, and J. Chen, "A family of cost-efficient non-isolated single-inductor three-port converters for low power stand-alone renewable power applications," in *Conference Proceedings - IEEE Applied Power Electronics Conference and Exposition - APEC*, IEEE, 2013, pp. 1083–1088. doi: 10.1109/APEC.2013.6520434.

[15] Y. Chen *et al.*, "Dynamical modelling of the non-isolated single-inductor three-port converter," in *2014 IEEE Applied Power Electronics Conference and Exposition (APEC)*, IEEE, 2014.

[16] N. Vazquez and others, "A three-port converter for renewable energy applications," in *2011 IEEE International Symposium on Industrial Electronics*, IEEE, 2011.

[17] Z. Zhou, H. Wu, X. Ma, and Y. Xing, "A non-isolated three-port converter for stand-alone renewable power system," in *IECON Proceedings (Industrial Electronics Conference)*, IEEE, 2012, pp. 3352–3357. doi: 10.1109/IECON.2012.6389360.

[18] G. Wen, Y. Chen, and Y. Kang, "A family of cost-efficient integrated single-switch three-port converters," in *2013 Twenty-Eighth Annual IEEE Applied Power Electronics Conference and Exposition (APEC)*, IEEE, 2013.

[19] H. Zhu, D. Zhang, B. Zhang, and Z. Zhou, "A non-isolated three-port DC-DC converter and three-domain control method for PV-battery power systems," *IEEE Transactions on Industrial Electronics*, vol. 62, no. 8, pp. 4937–4947, 2015, doi: 10.1109/TIE.2015.2393831.

[20] Y. M. Chen, A. Q. Huang, and X. Yu, "A high step-up three-port DC-DC converter for stand-alone PV/battery power systems," *IEEE Transactions on Power Electronics*, vol. 28, no. 11, pp. 5049–5062, 2013, doi: 10.1109/TPEL.2013.2242491.

[21] Y. M. Chen, X. Yu, and A. Q. Huang, "A new non-isolated three-port dc-dc converter with high step-up/down ratio," in *2012 IEEE Energy Conversion Congress and Exposition, ECCE 2012*, IEEE, 2012, pp. 1520–1526. doi: 10.1109/ECCE.2012.6342633.
[22] L.-J. Chien and others, "Novel three-port converter with high-voltage gain," *IEEE Transactions on Power Electronics*, vol. 29, no. 9, pp. 4693–4703, 2013.
[23] Y. M. Chen, Y. C. Liu, and F. Y. Wu, "Multi-input dc/dc converter based on the multilinking transformer for renewable energy applications," *IEEE Transactions on Industry Applications*, vol. 38, no. 4, pp. 1096–1104, 2002, doi: 10.1109/TIA.2002.800776.
[24] C. Zhao, S. D. Round, and J. W. Kolar, "An isolated three-port bidirectional dc-dc converter with decoupled power flow management," *IEEE Transactions on Power Electronics*, vol. 23, no. 5, pp. 2443–2453, 2008, doi: 10.1109/TPEL.2008.2002056.
[25] L. Piris-Botalla, G. G. Oggier, and G. O. García, "Extending the power transfer capability of a three-port DC-DC converter for hybrid energy storage systems," *IET Power Electronics*, vol. 10, no. 13, pp. 1687–1697, 2017, doi: 10.1049/iet-pel.2016.0422.
[26] B. Chen, Y. Wang, P. Wang, W. Li, F. Han, and L. Yang, "An improved analysis method of loss for the lclc multi-resonant three-port bidirectional dc-dc converter," in *Conference Proceedings - IEEE Applied Power Electronics Conference and Exposition - APEC*, IEEE, 2018, pp. 2129–2134. doi: 10.1109/APEC.2018.8341311.
[27] B. Parida, S. Iniyan, and R. Goic, "A review of solar photovoltaic technologies," *Renewable and Sustainable Energy Reviews*, vol. 15, no. 3, pp. 1625–1636, 2011, doi: 10.1016/j.rser.2010.11.032.
[28] M. Hosenuzzaman, N. A. Rahim, J. Selvaraj, M. Hasanuzzaman, A. B. M. A. Malek, and A. Nahar, "Global prospects, progress, policies, and environmental impact of solar photovoltaic power generation," *Renewable and Sustainable Energy Reviews*, vol. 41, pp. 284–297, 2015, doi: 10.1016/j.rser.2014.08.046.
[29] Z. Rehman, I. Al-Bahadly, and S. Mukhopadhyay, "Multiinput DC-DC converters in renewable energy applications - an overview," *Renewable and Sustainable Energy Reviews*, vol. 41, pp. 521–539, 2015, doi: 10.1016/j.rser.2014.08.033.
[30] F. Ahmeti and D. Arnaudov, "Energy flows management of a multi-port dc-dc converter for an energy storage system," in *13th National Conference with International Participation, ELECTRONICA 2022 - Proceedings*, IEEE, 2022. doi: 10.1109/ELECTRONICA55578.2022.9874370.
[31] J. L. Duarte, M. Hendrix, and M. G. Simões, "Three-port bidirectional converter for hybrid fuel cell systems," *IEEE Transactions on Power Electronics*, vol. 22, no. 2, pp. 480–487, 2007, doi: 10.1109/TPEL.2006.889928.
[32] C. Zhao, S. D. Round, and J. W. Kolar, "An isolated three-port bidirectional DC-DC converter with decoupled power flow management," *IEEE Transactions on Power Electronics*, vol. 23, no. 5, pp. 2443–2453, 2008, doi: 10.1109/TPEL.2008.2002056.
[33] G. G. Oggier, L. Piris Botalla, and G. O. García, "Soft-switching analysis for three-port bidirectional dc-dc converters," in *2010 9th IEEE/IAS International Conference on Industry Applications (INDUSCON)*, IEEE, 2010.
[34] L. Piris-Botalla, G. G. Oggier, A. M. Airabella, and G. O. García, "Analysis and evaluation of power switch losses for three-port bidirectional dc-dc converter," in *2012 IEEE International Conference on Industrial Technology, ICIT 2012, Proceedings*, IEEE, 2012, pp. 950–955. doi: 10.1109/ICIT.2012.6210061.
[35] L. Piris-Botalla, G. G. Oggier, A. M. Airabella, and G. O. García, "Power losses evaluation of a bidirectional three-port dc-dc converter for hybrid electric system," *International Journal of Electrical Power and Energy Systems*, vol. 58, pp. 1–8, 2014, doi: 10.1016/j.ijepes.2013.12.021.
[36] M. Phattanasak, R. Gavagsaz-Ghoachani, J. P. Martin, B. Nahid-Mobarakeh, S. Pierfederici, and B. Davat, "Control of a hybrid energy source comprising a fuel cell and two storage devices using isolated three-port bidirectional dc-dc converters," *IEEE Transactions on Industry Applications*, vol. 51, no. 1, pp. 491–497, 2015, doi: 10.1109/TIA.2014.2336975.
[37] B. Hoxha, R. Selimaj, D. Krasniqi, and S. Osmanaj, "Cogeneration of energy in solar systems-a study case, Kosovo," *International Journal of Power Electronics and Drive Systems*, vol. 10, no. 3, pp. 1675–1686, 2019, doi: 10.11591/ijpeds.v10.i3.pp1675-1686.
[38] N. Zhang, D. Sutanto, and K. M. Muttaqi, "A review of topologies of three-port DC-DC converters for the integration of renewable energy and energy storage system," *Renewable and Sustainable Energy Reviews*, vol. 56, pp. 388–401, 2016, doi: 10.1016/j.rser.2015.11.079.
[39] S. Arulmozhi and K. R. Santha, "Review of multiport isolated bidirectional converter interfacing renewable and energy storage systems," *International Journal of Power Electronics and Drive Systems*, vol. 11, no. 1, pp. 466–476, 2020, doi: 10.11591/ijpeds.v11.i1.pp466-467.
[40] S. Y. Kim, H. S. Song, and K. Nam, "Idling port isolation control of three-port bidirectional converter for EVs," *IEEE Transactions on Power Electronics*, vol. 27, no. 5, pp. 2495–2506, 2012, doi: 10.1109/TPEL.2011.2172225.
[41] M. Phattanasak, R. Gavagsaz-Ghoachani, J. P. Martin, S. Pierfederici, and B. Davat, "Flatness based control of an isolated three-port bidirectional dc-dc converter for a fuel cell hybrid source," in *IEEE Energy Conversion Congress and Exposition: Energy Conversion Innovation for a Clean Energy Future, ECCE 2011, Proceedings*, IEEE, 2011, pp. 977–984. doi: 10.1109/ECCE.2011.6063878.
[42] H. Krishnaswami and N. Mohan, "Three-port series-resonant DC-DC converter to interface renewable energy sources with bidirectional load and energy storage ports," *IEEE Transactions on Power Electronics*, vol. 24, no. 10, pp. 2289–2297, 2009, doi: 10.1109/TPEL.2009.2022756.
[43] S. Falcones and R. Ayyanar, "Simple control design for a three-port DC-DC converter-based PV system with energy storage," in *Conference Proceedings - IEEE Applied Power Electronics Conference and Exposition - APEC*, IEEE, 2010, pp. 2149–2153. doi: 10.1109/APEC.2010.5433534.
[44] M. Forouzesh, Y. P. Siwakoti, S. A. Gorji, F. Blaabjerg, and B. Lehman, "Step-up DC-DC converters: a comprehensive review of voltage-boosting techniques, topologies, and applications," *IEEE Transactions on Power Electronics*, vol. 32, no. 12, pp. 9143–9178, 2017, doi: 10.1109/TPEL.2017.2652318.
[45] I. N. Jiya, A. Salem, H. van Khang, and R. Pomarnacki, "Integrated multiport DC-DC and multilevel converters for multiple renewable energy source integration," *IEEE Access*, vol. 11, pp. 132483–132495, 2023, doi: 10.1109/ACCESS.2023.3336567.
[46] S. Gopinathan, V. S. Rao, and K. Sundaramoorthy, "Family of non-isolated quadratic high gain dc-dc converters based on extended capacitor-diode network for renewable energy source integration," *IEEE Journal of Emerging and Selected Topics in Power Electronics*, vol. 10, no. 5, pp. 6218–6230, 2022, doi: 10.1109/JESTPE.2022.3167283.
[47] D. Ertekin, "A high gain switched-inductor-capacitor dc-dc boost converter for photovoltaic-based micro-grid applications," *CSEE Journal of Power and Energy Systems*, vol. 10, no. 6, pp. 2398–2410, 2024, doi: 10.17775/CSEEJPES.2022.08440.
[48] T. Sutikno, A. S. Samosir, R. A. Aprilianto, H. S. Purnama, W. Arsadiando, and S. Padmanaban, "Advanced DC-DC converter topologies for solar energy harvesting applications: a review," *Clean Energy*, vol. 7, no. 3, pp. 555–570, 2023, doi: 10.1093/ce/zkad003.
[49] L. Guo, X. Chen, J. Chen, P. Luo, and L. Zhao, "CLLCLC topology based on adaptive excitation inductance for the improvement of bidirectional dc-dc converter efficiency," *IEEE Access*, vol. 11, pp. 137594–137605, 2023, doi: 10.1109/ACCESS.2023.3329965.

[50] I. N. Jiya, H. Van Khang, P. Gunawardena, N. Kishor, and Y. R. Li, "Novel isolated multiport dc converter with natural bipolar symmetry for renewable energy source integration to dc grids," *IEEE Access*, vol. 11, pp. 117729–117740, 2023, doi: 10.1109/ACCESS.2023.3326752.

BIOGRAPHIES OF AUTHORS

Faruk Ahmeti is a teaching assistant since 2022 in the Faculty of Electrical and Computer Engineering (FECE) in University of Prishtina, Prishtina, Kosovo. He is also a Project Manager in a local company in Kosovo for Photovoltaic Solar Systems. He is doing his Ph.D. studies in distance learning for power electronics at the Technical University of Sofia, Sofia, Bulgaria. He received his B.Eng. degree in Electrical Engineering from the University of Prishtina, and his M.Eng. degree in Electronics from Istanbul Sehir University, Istanbul, Türkiye. His research interests include the field of digital design, industrial applications, industrial electronics, industrial informatics, power electronics, renewable energy, and MEMS/NEMS. He can be contacted at email: faruk.ahmeti@uni-pr.edu.

Dimitar Arnaudov was born in Smolyan, Bulgaria, in 1974. He received the M.S. and Ph.D. degrees in electronic engineering from the Technical University of Sofia, Sofia, Bulgaria, in 1998 and 2003. In 2001, he joined the Department of Telecommunication, Higher College of Telecommunication and Posts, Sofia, as an assistant professor. He joined the Faculty of Electronic Engineering and Technologies at Technical University-Sofia, Sofia, in 2009, where he is an associate professor in the Department of Power Electronics. His interests include power electronics, industrial electronics, power supplies, induction heating, and renewable energy sources. He is a member of the Union of Electronic, Electrical Engineering and Telecommunications (CEEC) in Bulgaria. CEEC is a member of the Convention of National Societies of Electrical Engineers in Europe (EUREL). He can be contacted at email: dda@tu-sofia.bg.

Sabrije Osmanaj is a lecturer in the Department of Electronic, Automatic, and Robotic Engineering at the University of Prishtina, Kosovo, since 2002, and a senior lecturer since 2011. She earned her B.Eng. degree in Electrical Engineering and her M.Eng. degree in Electronics from the University of Prishtina in 1996 and 2003, respectively. In 2009, she obtained her Ph.D. from the Faculty of Electrical Engineering at the Polytechnic University of Tirana, Albania. She has contributed to numerous projects, and her research interests encompass power electronics, motor drives, industrial applications, industrial electronics, photovoltaic power systems, and digital design. She can be contacted at email: sabrije.osmanaj@uni-pr.edu.